

## Structural safety redundancy-based design method for structure with viscous dampers

Linfei Hao<sup>1,2a</sup> and Ruifu Zhang<sup>\*1</sup>

<sup>1</sup>Research Institute of Structural Engineering and Disaster Reduction, Tongji University,  
Shanghai 200092, China

<sup>2</sup>Department of Architecture, Tohoku University, Sendai 980-8579, Japan

(Received November 3, 2015, Revised March 27, 2016, Accepted April 5, 2016)

**Abstract.** A simple design process is proposed for supplemental viscous dampers based on structural safety redundancy. In this process, the safety redundancy of the primary structure without a damper is assessed by the capacity and response spectra. The required damping ratio that should be provided by the supplemental dampers is estimated by taking the structural safety redundancy as a design target. The arrangement of dampers is determined according to the drift distribution obtained by performing pushover analysis. A benchmark model is used to illustrate and verify the validity of this design process. The results show that the structural safety redundancy of the structure provided by the viscous dampers increases to approximately twice that of the structure without a damper and is close to the design target. Compared with the existing design methods, the proposed process can estimate the elastic-plastic response of a structure more easily by using static calculation, and determine the required damping ratio more directly without iterative calculation or graphical process. It can be concluded that the proposed process is simple and effective.

**Keywords:** structural safety redundancy; viscous damper; elastic-plastic design; seismic spectrum

### 1. Introduction

An effective method to improve the seismic performance of a structure is to increase the damping ratio by adding a viscous damper (Kasai and Matsuda 2014, Miyamoto *et al.* 2010, Huang 2009, Chang *et al.* 2008, Hamidia *et al.* 2015). At the same time, Performance-based seismic design (PBSD) (Ghobarah 2001) has been incorporated in a variety of design codes including the design of structures with dampers (ABCA 1996, BIA 1995, ECE 1996). Generally, the PBSD process for a structure equipped with viscous dampers consists of the following steps: (a) Assess whether the seismic performance of a structure without a damper (SWOD) can meet the requirements to withstand the target earthquake. (b) According to the assessment result and design performance target, calculate the required damping ratio that should be provided by viscous dampers. (c) Determine the parameters and location of dampers to be installed. (d) Check whether

---

\*Corresponding author, Assistant Professor, E-mail: [zhangruifu@tongji.edu.cn](mailto:zhangruifu@tongji.edu.cn)

<sup>a</sup>Ph.D. Candidate, E-mail: [hao@rcl.archi.tohoku.ac.jp](mailto:hao@rcl.archi.tohoku.ac.jp)

the seismic performance of the structure with a damper (SWD) meets the performance target.

The design method of an SWD in the elastic range has been discussed by many researchers (Gluck *et al.* 1996, Singh and Moereschi 2002, Zhang and Soong 1992, Suarez and Gaviria 2015). For minor earthquakes and wind vibration, the elastic design method is effective. However, according to PBSD requirements, a structure should meet performance targets of different earthquake levels ranging from a minor earthquake to a severe one. If a structure is allowed to enter the plastic range during a severe earthquake, a design covering only the elastic range cannot ensure performance targets in the plastic range. The economic efficiency of the structure will be poor if the structure is assumed to be in the elastic range even during a severe earthquake.

The time history method is a feasible elastic-plastic design method (Chopra 2007, Weng *et al.* 2012). This method can consider the elastic-plastic response of a structure, and hence can approximately simulate the actual situation of a structure experiencing a severe earthquake. Satisfactory parameters and suitable locations for the dampers can be found by a trial-and-error process. However, this obviously requires large amounts of computing resources and time.

A simpler method to predict the structural elastic-plastic seismic response involves using the capacity spectrum method (Chopra and Goel 1999, Fajfar 1999), along with the pushover analysis (ATC 1996, FEMA 1997). The elastic-plastic behavior of a structure is represented by the capacity spectrum of a single-degree-of-freedom (SDOF) system. By using pushover analysis and the response spectrum, dynamic analysis can be simplified to a static calculation. Some researchers proposed design methods for the supplemental dampers based on the capacity spectrum method (Kim *et al.* 2003, Kim and Choi 2006, Lin *et al.* 2003). In these methods, the capacity spectrum method is used to assess the response of the structure under a target seismic load, and the required damping ratio that should be provided by the supplemental dampers is estimated according to the seismic response. Then, the dampers are designed according to the required damping ratio. Generally, the graphical method and iterative calculations are needed to determine the structural response.

In this paper, a simpler method is proposed by using which a damper can be designed more directly based on the structural safety redundancy, which refers to the redundancy of structural safety limit corresponding to the structural seismic response. After the capacity spectrum of a structure is obtained by pushover analysis, the response reduction factor (RRF) and seismic redundancy indicator (SRI) are used to evaluate the redundancy of the target structural performance points (SPPs) corresponding to the seismic response. Then, the required damping ratio can be determined by considering the SRI as a design target so that the structure can acquire the expected seismic redundancy. The location and number of dampers are decided according to the distribution of the story drift obtained by pushover analysis, and then, the damping force of the dampers are determined. In the actual design, viscous damper products can be chosen based on the design damping force. A 12-story reinforced concrete (RC) frame is chosen to illustrate the proposed process, and time history analysis is used to verify the validity.

## 2. Structural safety redundancy

### 2.1 Capacity spectrum and SPP

To draw the capacity spectrum of a structure, pushover analysis needs to be conducted first. As shown in Fig. 1, the relationship between the story shear force  $q_i$  and relative story displacement  $d_i$

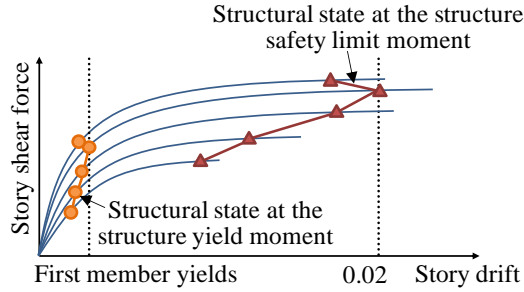


Fig. 1 Performance limit states reflected on  $q_i-\Delta_i$  curves

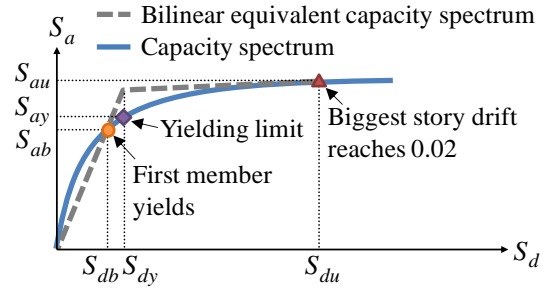


Fig. 2 Determination of yielding limit using energy equivalent method

can be obtained by performing pushover analysis. At each moment during the evolution of the structural capacity (corresponding to each step in the pushover analysis), the  $q_i-d_i$  relationship of all the stories corresponds to a group of points. Using Eqs. (1)-(4), the  $q_i-d_i$  curves can be reduced to an  $S_a-S_d$  curve, which means that an MDOF system can be simplified to an SDOF elastic-plastic system, as shown in Fig. 2 (ATC 1996). The  $S_a-S_d$  curve of the equivalent SDOF system is called as the capacity spectrum of the structure.

$$S_a = \frac{q_1}{M^*} \quad (1)$$

$$S_d = \frac{\Delta_n}{\gamma_1 \times \varphi_{n,1}} \quad (2)$$

$$M^* = \frac{\left[ \sum (m_i \times \varphi_{i,1}) \right]^2}{\sum (m_i \times \varphi_{i,1}^2)} \quad (3)$$

$$\gamma_1 = \frac{\sum (m_i \times \varphi_{i,1})}{\sum (m_i \times \varphi_{i,1}^2)} \quad (4)$$

$$T = 2\pi \sqrt{\frac{S_d}{S_a}} \quad (5)$$

where  $q_1$  is the base shear force,  $M^*$  is the equivalent mass,  $m_i$  is the mass of the  $i$ th story,  $\gamma_1$  is the modal participation factor in the first mode,  $\varphi_{i,1}$  is the modal displacement of the  $i$ th story (the  $i$ th mass in the MDOF system) in the first mode,  $\varphi_{1,1}$  is the modal displacement at the top of the structure in the first mode, and  $\Delta_n$  is the displacement at the top of the structure. The equivalent period  $T$  of each point on the capacity spectrum  $T$  can be obtained by using Eq. (5),

Pushover analysis can reflect the overall process of structural performance evolution from individual members to the entire structure, and the capacity spectrum can be acquired from a group of  $q_i-d_i$  curves obtained from the pushover analysis. Thus, each point of the capacity spectrum corresponds to each step of the structural performance state in the pushover analysis. A point on the capacity spectrum is defined as an SPP. Generally, in PBS, some critical structural performance states are considered as performance targets, and the SPP of the structural critical

performance state is defined as the critical SPP.

After the capacity spectrum of the equivalent SDOF system is determined, the displacement of the yielding limit SPP  $S_{dy}$  can be obtained by using the energy equivalent method as follows. As shown in Fig. 1, the safety limit state, which corresponds to the safety limit SPP ( $S_{du}$ ,  $S_{au}$ ) of the capacity spectrum (Fig. 2), is considered as the state in which the maximum inter-story drift reaches 0.02. In addition, the SPP corresponding to the step at which the first member yields (Fig. 1) is considered as the initial plastic SPP ( $S_{db}$ ,  $S_{ab}$ ) of the capacity spectrum (Fig. 2). Then, an area equivalent bilinear curve is determined and used to decide the yielding limit  $S_{dy}$  on the capacity spectrum (Fig. 2). The bilinear curve passes through the starting point, safety limit SPP, and initial plastic SPP of the capacity spectrum. The yielding limit SPP ( $S_{dy}$ ,  $S_{ay}$ ) of the capacity spectrum can be decided according to the yielding point of the bilinear curve, as shown in Fig. 2.

## 2.2 Response spectrum

The seismic response spectrum is a function of the peak response of the elastic SDOF system and its period  $T$ . In general, a standard response spectrum consists of rising, horizontal, and declining segments and can be expressed by a piecewise function such as Eq. (6)

$$\begin{cases} S_{a0}(T) = f_1(T), & T \leq T_0 \\ S_{a0}(T) = S_{a,\max}, & T_0 < T \leq T_g \\ S_{a0}(T) = f_3(T), & T > T_g \end{cases} \quad (6)$$

For the elastic SDOF system, the following relationship exists among the acceleration response  $S_a$ , displacement response  $S_d$ , and period  $T$

$$S_a = \left( \frac{2\pi}{T} \right)^2 S_d \quad (7)$$

According to Eq. (7), the response spectrum can be transferred into a  $S_a$ – $S_d$  spectrum, as shown in Fig. 3. For each point on the response spectrum in Fig. 3, the relationship between  $S_a$  and  $S_d$  represents the acceleration and displacement responses of an elastic SDOF system with period  $T$ .

## 2.3 EDR and RRF

In Fig. 3, only material damping is considered for the standard response spectrum. The material

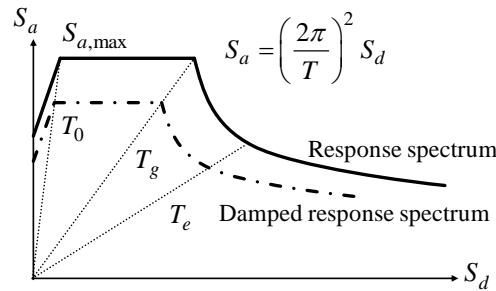


Fig. 3 Response spectra expressed in  $S_a$ – $S_d$  coordinates

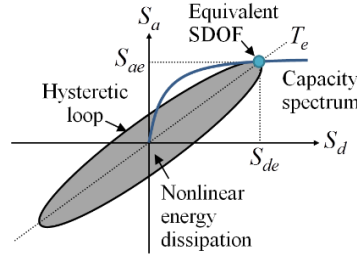


Fig. 4 Equivalent SDOF system and hysteretic energy dissipation

damping ratio of an RC structure is generally 5%. Each SPP on the capacity spectrum shown in Fig. 4 can be seen as an equivalent elastic SDOF system. The seismic capacity of the equivalent elastic SDOF system is represented by the coordinates of the SPP ( $S_{ae}$ ,  $S_{de}$ ), and the equivalent period  $T_e$  can be obtained using Eq. (5). The elastic seismic response of the equivalent SDOF system can be decided according to the period on the standard response spectrum (Fig. 3). However, considering the plastic response of the structure and the hysteretic loop in Fig. 4, additional hysteretic damping should be included to determine the real structural response.

The hysteretic damping can be considered by the equivalent damping ratio (EDR), and the EDR of the structure  $\xi_s$  can be expressed as a function of the structural plasticity coefficient  $\mu$  (Gulkan and Sozen 1974)

$$\xi_s = \xi_0 + 0.2 \left( 1 - \frac{1}{\sqrt{\mu}} \right) \quad (8)$$

where  $\xi_0$  is the material damping ratio. When  $\mu < 1$ ,  $\xi_s = \xi_0$ . For an SPP on the capacity spectrum, when  $S_d$  is greater than  $S_{dy}$  (Fig. 2), the plasticity coefficient  $\mu$  can be written as

$$\mu = \frac{S_d S_{ay}}{S_{dy} S_a} \quad (9)$$

The reduction of seismic response because of the additional damping can be considered by modifying the standard response spectrum according to the EDR (ATC 1996) or by multiplying the standard response spectrum by the RRF (MLIT 1998). This consideration is specified in the Japanese Building Code as follows (AIJ 2004)

$$S_{ar} = D_h S_{a0} \quad (10)$$

where  $S_{a0}$  is the acceleration response of the standard response spectrum and  $S_{ar}$  is the acceleration of the response spectrum after reduction. The RRF  $D_h$  can be expressed as

$$D_h = \frac{1.5}{1 + 10\xi} \quad (11)$$

When the contribution of viscous dampers is considered, the total EDR of the structure  $\xi$  can be written as

$$\xi = \xi_s + \xi_r = \xi_0 + 0.2 \left( 1 - \frac{1}{\sqrt{\mu}} \right) + \xi_r \quad (12)$$

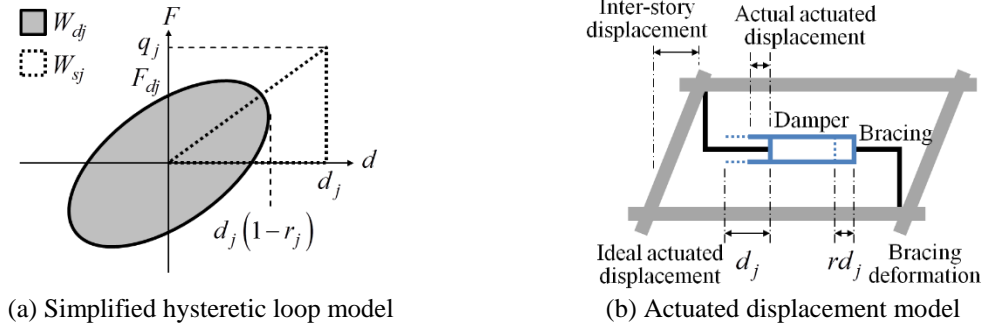


Fig. 5 Model of hysteretic loop and actuated displacement of viscous damper

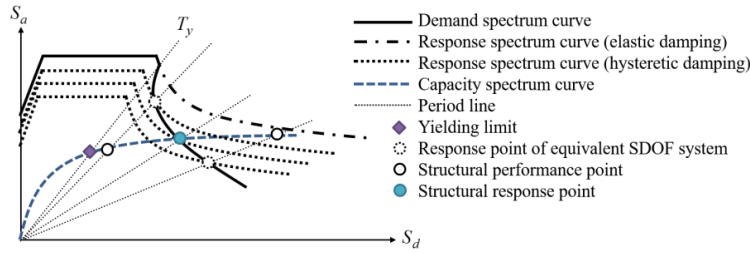


Fig. 6 Definition of demand spectrum

According to the physical significance of the EDR, the EDR of the viscous damper  $\xi$  (Fig. 5 (a)) can be calculated as follows (Chopra 2007)

$$\xi_r = \frac{\sum W_{dj}}{\sum 4\pi W_{sj}} = \frac{4 \sum [F_{dj} d_j (1 - r_j)]}{4\pi \times \frac{1}{2} \sum (d_j q_j)} = \frac{2 \sum [F_{dj} d_j (1 - r_j)]}{\pi \sum (d_j q_j)} \quad (13)$$

where  $W_{dj}$  is the energy dissipation of the viscous damper installed at the  $j$ th floor,  $W_{sj}$  is the strain energy of the  $j$ th floor,  $F_{dj}$  is the damping force of the damper at the  $j$ th floor,  $d_j$  is the inter-story displacement of the  $j$ th floor, and  $q_j$  is the story shear force of the  $j$ th floor. Generally, the displacement of the damper is not equal to the inter-story displacement because of the deformation of the steel brace.  $r_j$  is the ratio of the relative displacement of the steel brace to the inter-story displacement, and  $d_j(1-r_j)$  is the actuated displacement of the damper piston rod at the  $j$ th floor (Fig. 5 (b)).

#### 2.4 Structural response point (SRP) and SRI

As shown in Fig. 4, each SPP can be regarded as an equivalent elastic SDOF system, and the seismic response can be obtained on the response spectrum (Fig. 3) according to its equivalent period. By considering the additional damping provided by the hysteretic response (Eq. (12)), the total EDR of SWD is obtained. As shown in Fig. 6,  $T_y$  is the equivalent period of the yielding limit SPP. When  $T$  of an SPP is greater than  $T_y$ , as  $\mu$  increases, the EDR and  $D_h$  decrease, according to Eq. (8) and Eq. (11); thus, the response spectrum is reduced progressively (Eq. (10)). The seismic response of each of the equivalent SDOF systems can be decided on the reduced response spectra

according to their equivalent period and EDR. By connecting the response points of each of the equivalent SDOF systems corresponding to each of the SPPs on the capacity spectrum, the demand spectrum can be determined.

As shown in Fig. 6, the demand spectrum generally intersects with the capacity spectrum, and this intersection is defined as the SRP, which corresponds to the structural response state.

Existing design methods for the viscous damper (Kim *et al.* 2003, Kim and Choi 2006, Lin *et al.* 2003) require iterative calculations to determine the SRP by the graphical method. However, the purpose of the design is to ensure that the seismic response of the object structure does not exceed a certain safety limit state, which implies that only the redundancy of the safety limit SPP corresponding to the seismic response should be ensured to be greater than 1.0 and the exact location of the SRP need not be determined. On the other hand, because of the randomness of the seismic ground motion and structural response, it is impossible that the actual seismic response would exactly coincide with the SRP. Therefore, it is unnecessary to determine the SRP exactly by the graphical method and iterative calculations in the design.

To describe the safety redundancy of the structure, the SRI  $\alpha$  is defined as the ratio of the safety limit SPP to the response point of the corresponding equivalent SDOF system (Fig. 7)

$$\alpha = \frac{S_{du}}{S_{dr}} = \frac{S_{au}}{S_{ar}} \quad (14)$$

In Fig. 6, if  $\alpha > 1$ , the SRP of the object structure does not exceed the safety limit SPP. If  $\alpha < 1$ , the SRP exceeds the safety limit SPP. If  $\alpha = 1$ , the structural seismic response is at the safety limit SPP.

The SRI  $\alpha$  is considered as a quantitative performance indicator in the proposed design process. As shown in Fig. 8, if the SRI  $\alpha$  of the SWOD is smaller than 1.0, the safety redundancy

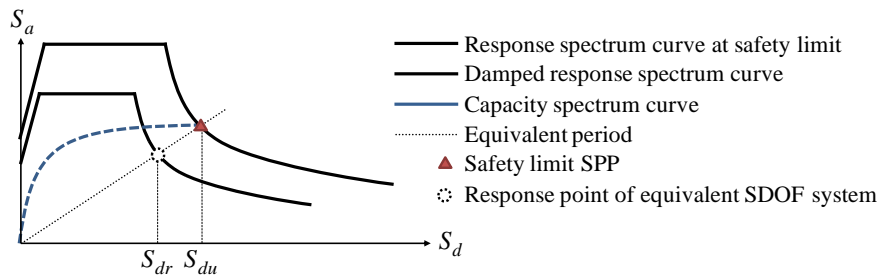


Fig. 7 Definition of the safety redundancy indicator (SRI)

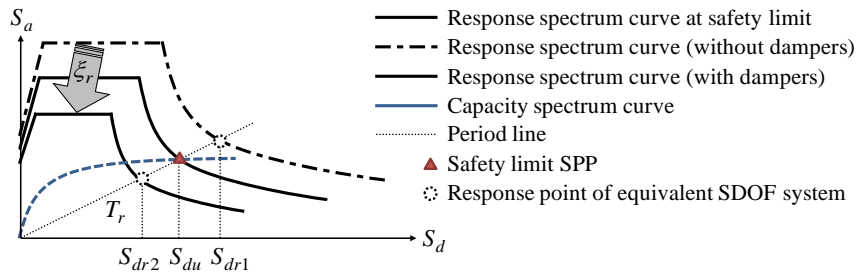


Fig. 8 Influence of required EDR  $\zeta_r$

requirement cannot be satisfied. Considering the SRI of the SWD as the design target, by setting  $\alpha > 1$ , the required RRF  $D_h$ , entire EDR of the SWD  $\xi$ , and required EDR  $\xi_r$  provided by the supplemental viscous damper can be obtained. Thus, the SWD can be designed according to the required EDR  $\xi_r$ .

### 3. Design principle of damaged structure

The flowchart of this design process is shown in Fig. 9. And the detailed design process is presented below:

Step 1: Obtain the capacity spectrum of the SWOD, safety limit SPP, and EDR  $\xi_s$  corresponding to the safety limit SPP. Pushover analysis is performed on the object SWOD, and the capacity spectrum is obtained based on the  $q_i-d_i$  curves according to Eqs. (1)-(4). The initial yielding limit SPP ( $S_{db}$ ,  $S_{ab}$ ) and safety limit SPP ( $S_{du}$ ,  $S_{au}$ ) are obtained according to their definitions (Fig. 1). The displacement of the yielding limit SPP ( $S_{dy}$ ,  $S_{ay}$ ) is decided by the energy equivalent method. Then, the structural EDR  $\xi_s$  and plasticity coefficient  $\mu$  corresponding to the safety limit SPP are obtained according to Eqs. (8) and (9), respectively.

Step 2: Determine the stories at which viscous dampers should be installed. The story drift distribution obtained by performing pushover analysis at the safety limit state is used to decide the number and location of the dampers. Generally speaking, it is economical to install the dampers at the stories having relatively large story drifts and stories that exceed the safety limit (0.02) first, so that the actuated distance of the viscous damper is longer and the energy dissipation performance may be better. The value obtained in Eq. (15) describes the deviation between the story drift of a certain story and the average story drift at the safety limit state.

$$\frac{d_i/h_i}{(d_i/h_i)} \geq \gamma_u \quad (15)$$

where  $d_i$  and  $h_i$  denote the story drift and height of the  $i$ th story, respectively.  $\gamma_u$  denotes the relative value of the  $i$ th story drift to the average story drift. When  $\gamma_u$  exceeds 1.0, some stories with relatively large story drifts are selected to be installed with viscous dampers.  $\gamma_u$  should be adjusted and determined comprehensively according to the force of the damper, installation cost, and distribution of dampers.

Step 3: Assume the EDR provided by the supplemental dampers. Based on the distribution of the inter-story displacement at the safety limit state, the damping force of each story  $F_{dj}$  is expressed as

$$F_{dj} = f_d \frac{d_j}{\bar{d}_j} \quad (16)$$

where  $f_d$  is a damping force parameter,  $d_j$  is the inter-story displacement, and  $\bar{d}_j$  is the average inter-story displacement. Therefore, it is assumed that the damping forces provided in each story are proportional to the deviation of the inter-story displacement related to the average displacement. Then the design of the damping force  $F_{dj}$  of each story can be transferred to the design of the damping force parameter. The EDR provided by the supplemental viscous dampers can be obtained by using Eqs. (13) and (16) as follows



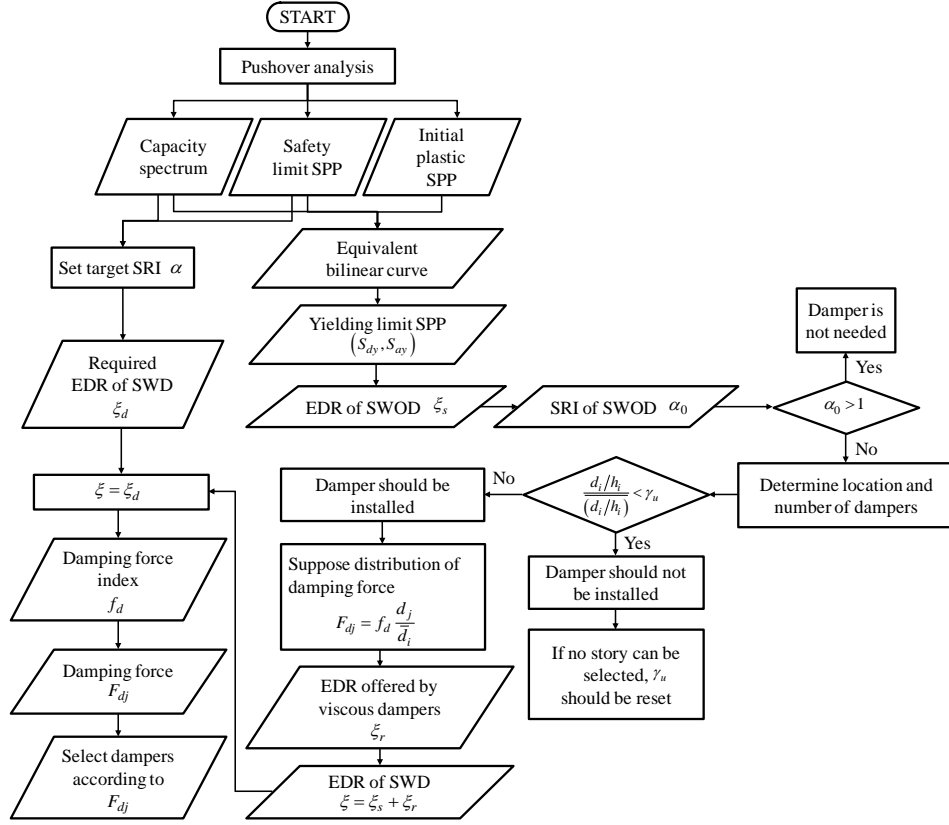


Fig. 9 Design flowchart for the supplemental viscous dampers

$$\xi_r = \frac{2 \sum [F_{dj} d_j (1 - r_j)]}{\pi \sum (d_j q_j)} = \frac{2 f_d \sum [d_j^2 (1 - r_j) / \bar{d}_i]}{\pi \sum (d_j q_j)} \quad (17)$$

Step 4: Determine the required EDR and damping force provided by the supplemental viscous dampers. Based on Eqs. (5), (10) and (14), the following relationships can be obtained

$$\alpha = \frac{S_{au}}{S_{ar}} = \frac{S_{au}}{S_{a0}(T_u) \times D_h(\xi)} \quad (18)$$

$$T_u = 2\pi \sqrt{\frac{S_{du}}{S_{au}}} \quad (19)$$

where  $\alpha$  denotes the SRI corresponding to the safety limit SPP and  $T_u$  is the equivalent period corresponding to the safety limit SPP. Then, the entire EDR  $\xi_d$  required by the target SRI  $\alpha$  of the structural safety limit can be obtained according to Eqs. (11) and (18)

$$\xi_d = \frac{0.15}{D_h} - 0.1 = \frac{0.15 \alpha S_{a0}(T_u)}{S_{au}} - 0.1 \quad (20)$$

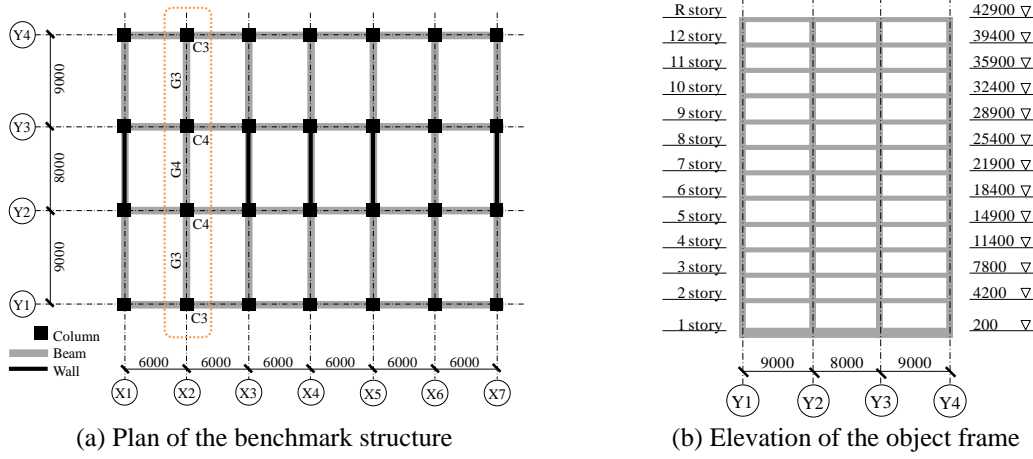


Fig. 10 The benchmark structure and the object frame

where  $\xi_d$  is the required EDR which ensures that the SRI of the structural safety limit satisfies the performance requirement.

The entire EDR of the SWD expressed by Eqs. (12) and (17) should be equal to the required entire EDR obtained by using Eq. (20),

$$\xi_d = \xi = \xi_s + \xi_r \quad (21)$$

Thus, the damping force parameter  $f_d$  can be expressed as follows

$$f_d = \frac{\pi \sum (d_j q_j)}{2 \sum [d_j^2 (1 - r_j) / \bar{d}_i]} \cdot (\xi_d - \xi_s) \quad (22)$$

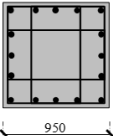
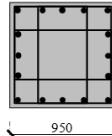
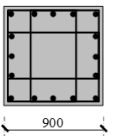
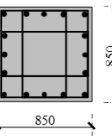
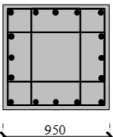
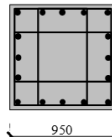
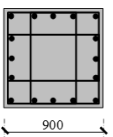
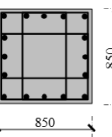
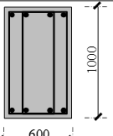
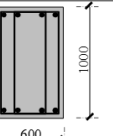
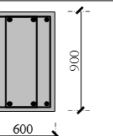
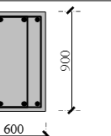
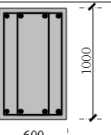
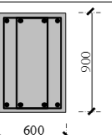
Then, the design damping force of each story equipped with dampers can be calculated according to Eq. (16) for a given value of  $f_d$ .

## 4. Design dexample

### 4.1 Model information

A benchmark 12-story RC structure adopted in the Japanese Guidelines for Performance Evaluation of Earthquake Resistant Reinforced Concrete Buildings (AIJ 2004) is used to illustrate and verify this proposed process. And the floor plan of the structure is shown in Fig. 10(a). A single frame along the X2 axis is analyzed in this study, and the elevation is shown in Fig. 10(b). The corresponding names and cross sections of each member are shown in Fig. 10(a) and Fig. 11. The mass of each story considered in the earthquake load (all the dead loads and part of the live loads are included) is listed in Table 1. The elastic damping ratio of the RC frame is 0.05.

The yielding strength of the steel bar is 390 MPa, and the compression strength of the concrete is 30 MPa. In the numerical analysis, the beams and columns are modeled using the strut model shown in Fig. 12.

Story	1~3	4~8	9, 10	11, 12
C3				
	Longitudinal bar	16-D41 <sup>a</sup>	16-D38	16-D35
	Stirrup	4-D13-@80 <sup>b</sup>	4-D13-@100	4-D13-@100
Story	1	2~8	9, 10	11, 12
C4				
	Longitudinal bar	16-D35	16-D35	16-D35
	Stirrup	4-D13-@80	4-D13-@100	4-D13-@100
Story	2~4		5~R	
G3	Outer	Inside	Outer	Inside
				
	Longitudinal bar		Longitudinal bar	
	Top: 4-D35; Bottom: 4-D35		Top: 4-D35; Bottom: 4-D35	
	Stirrup		Stirrup	
	4-D13-@150		4-D13-@150	
Story	2~4		5~R	
G4				
	Longitudinal bar		Longitudinal bar	
	Top: 4-D32; Bottom: 4-D32		Top: 4-D32; Bottom: 4-D32	
	Stirrup		Stirrup	
	4-D13-@150		4-D13-@150	

<sup>a</sup>16-D41: 16 steel bars with a diameter of 41 mm.

<sup>b</sup>4-D13-@80: 4 stirrups in both directions with a diameter of 13 mm and spacing of 150 mm.

Fig. 11 Member sections (AIJ 2004)

Table 1 Model Information (AIJ 2004)

Story	Story height (m)	Weight of seismic load $W_i$ (kN)	Total weight of seismic load $\Sigma W_i$ (kN)
12	3.50	2251	2251
11	3.50	2012	4263
10	3.50	2032	6295
9	3.50	2012	8307
8	3.50	2072	10378
7	3.50	2092	12470
6	3.50	2072	14542
5	3.50	2052	16593
4	3.50	2052	18645
3	3.60	2072	20717
2	3.60	2112	22828
1	4.00	2112	24940

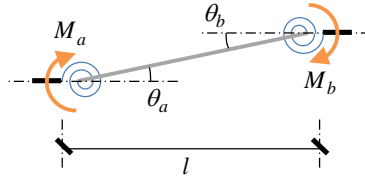


Fig. 12 Strut model for the beam and column

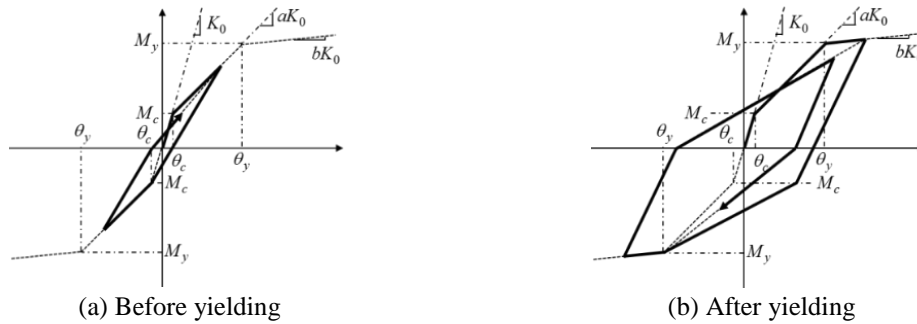


Fig. 13 Bending moment-rotation relationship for the beam and column

Assuming that bending yielding occurs at the ends of beams and columns, bending springs are placed at both ends of the strut models. Bending moment-rotation relationships of the bending springs are based on the trilinear model (Takeda *et al.* 1970) shown in Fig. 13, where  $M_c$  and  $M_y$  denote the cracking bending moment and yielding bending moment, respectively, and  $\theta_c$  and  $\theta_y$  represent the cracking rotation and yielding rotation of the members' section, respectively.  $K_0$ ,  $a$ , and  $b$  are the bending elastic stiffness, ratio of the cracked stiffness to the elastic stiffness, and ratio of the yielded stiffness to the elastic stiffness of the section, respectively.

In this study, viscous dampers are designed in term of the standard response spectrum in the Japanese MLIT code (MLIT 1998), and the acceleration response spectrum for the second ground site in the code can be expressed as

$$\begin{cases} S_{a0} = 480 + 4500T, & T \leq 0.16s \\ S_{a0} = 1200, & 0.16s < T \leq 0.864s \\ S_{a0} = 1036.8/T, & T > 0.864s \end{cases} \quad (23)$$

#### 4.2 Damper arrangement and design

Pushover analysis is performed, and the capacity spectrum of the equivalent SDOF system obtained by using Eqs. (1)-(4) is shown in Fig. 14. The yielding limit SPP is determined according to the energy equivalent bilinear curve. The yielding limit SPP ( $S_{dy}, S_{ay}$ ) is found to be (9.20 cm, 117.8 gal), and the safety limit SPP ( $S_{du}, S_{au}$ ) is found to be (40.34 cm, 148.1 gal). Then, the plasticity coefficient of the safety limit is determined to be 3.49 by using Eq. (9). The EDR of the SWOD  $\xi_s$  is determined to be 0.143 by using Eq. (8).

According to Eq. (19), the period of the equivalent SDOF system corresponding to the safety limit SPP  $T_u$  is determined to be 3.278 s. The corresponding acceleration response of the standard

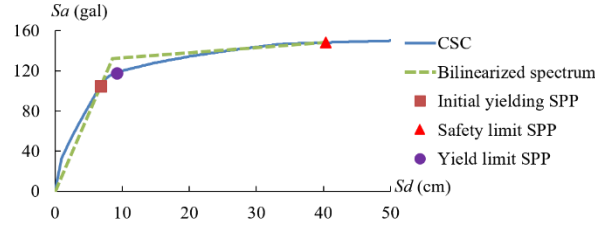


Fig. 14 Capacity spectrum, equivalent bilinear curve and the critical SPPs

Table 2 Pushover analysis results of SWOD at the safety limit state

Floor	1	2	3	4	5	6	7	8	9	10	11	12
Drift (pushover)	1/98	1/64	1/54	1/50	1/50	1/54	1/62	1/78	1/111	1/188	1/355	1/719
Displacement (pushover) $d_i$ (mm)	40.6	55.9	64.6	69.9	70.1	65.1	56.4	44.9	31.6	18.6	9.9	4.9
Shear force (pushover) $q_i$ (kN)	2978	2906	2808	2689	2545	2377	2180	1953	1697	1415	1090	711
Average of story drift							1/80					
Limit drift							1/67					
Stories requiring dampers							2, 3, 4, 5, 6, 7					

response spectrum  $S_{a0}$  is determined to be 316.3 gal, according to Eq. (23),

The response spectrum is reduced by discounting the standard curve according to Eqs. (10), (11), and (23). At the safety limit, the SRI  $\alpha$  is determined to be 0.76 according to Eq. (14), which means that the seismic response of the structure exceeds the safety limit. Hence, viscous dampers need to be installed to increase the entire EDR and ensure that the SRI of the safety limit satisfies the performance requirement.

At the safety limit state, the story drift distribution of the SWOD obtained by performing pushover analysis is listed in Table 2. Viscous dampers should be installed in the stories with relatively great inter-story displacements, which are selected by using Eq. (15). In this example, the deviation limit  $\gamma_u$  is set to 1.2, and the limit drift is determined to be 1/67. Therefore, the over-limit stories are Stories 2-7, in which the viscous dampers should be installed.

In this example, assuming that  $r_j$  in Eq. (17) is 0, the actuated displacement of the damper equals the inter-story displacement in Fig. 5(b),

The inter-story displacement  $d_j$ , average inter-story displacement  $\bar{d}_i$ , and story shear force  $q_j$  are already known (Table 2). By substituting these values and the obtained values of  $S_{au}$ ,  $S_{a0}$ , and EDR of the SWOD  $\xi_s$  into Eq. (22) and by setting the target SRI  $\alpha$  to be 1.7, the damping force parameters  $f_d$  can be obtained.

$$f_d = \frac{\pi \sum (d_j q_j)}{2 \sum [d_j^2 (1 - r_j) / \bar{d}_i]} \left\{ \frac{0.15 \alpha S_{a0} (T_u)}{S_{au}} - 0.1 - \xi_s \right\} = 1017 (\text{kN}) \quad (24)$$

The damping force of the damper and its actuated velocity can be expressed as

$$F = C V_y^r \quad (25)$$

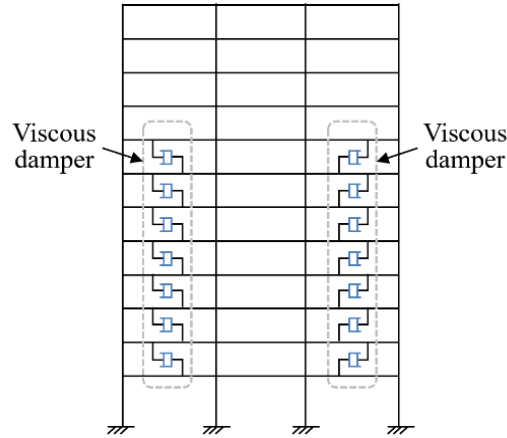


Fig. 15 Arrangement of the supplemental viscous dampers

Table 3 Parameters of the viscous damper

Story No.	2	3	4	5	6	7
Required damping force $F_{dj}$ (kN)	1077	1244	1338	1334	1233	1067
Number of dampers	2	2	2	2	2	2
Damping force of each damper $F$ (kN)	550	650	700	700	650	550
Damping coefficient $C$	400	400	400	400	400	400
Velocity factor $r$	0.25	0.25	0.25	0.25	0.25	0.25

Table 4 Seismic wave input

No.	Artificial/Natural	Name	Year	Direction	$M_w^*$	PGA (gal)	PGV (cm/s)	PGD (cm)
1	Artificial	BCJ-L1	—	—	—	207.3	30.3	49.2
2	Artificial	BCJ-L2	—	—	—	355.7	73.6	307.0
3	Natural	El Centro	1940	NS	6.4	341.7	33.5	10.9
4	Natural	Taft	1952	EW	7.7	175.9	17.7	9.2
5	Natural	Hachinohe	1968	EW	7.8	180.2	37.8	16.6
6	Natural	Tohoku	1978	NS	7.4	258.2	36.2	14.5
7	Natural	GEJE	2011	NS	9.0	333.0	49.3	103.5

$M_w$ : Moment magnitude; PGA: Peak ground acceleration; PGV: Peak ground velocity; PGD: Peak ground displacement.

where  $F$  is the damping force,  $C$  is the damping coefficient,  $V_y$  is the velocity of the damper piston rod when the damping force reaches the designed value, and  $r$  is the velocity index ( $0 < r < 1.0$ ). The parameters  $C$  and  $r$  are chosen according to the viscous dampers that can provide the required damping force.

Eq. (16) gives the required damping forces of Stories 2-7. As shown in Fig. 15, viscous dampers are set symmetrically along two sides of the frame and their actuating direction is set to be horizontal. The parameters of the viscous dampers are listed in Table 3.

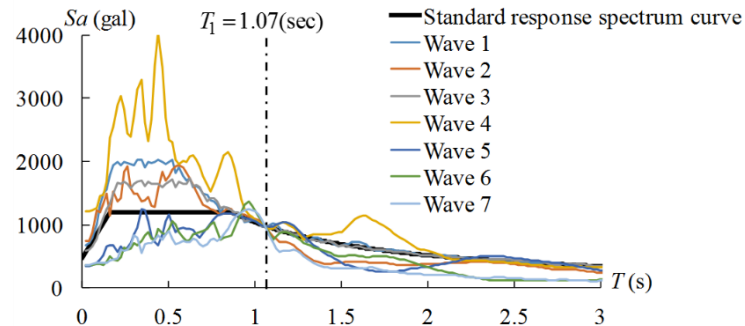


Fig. 16 Normalized acceleration response spectra of inputted seismic waves

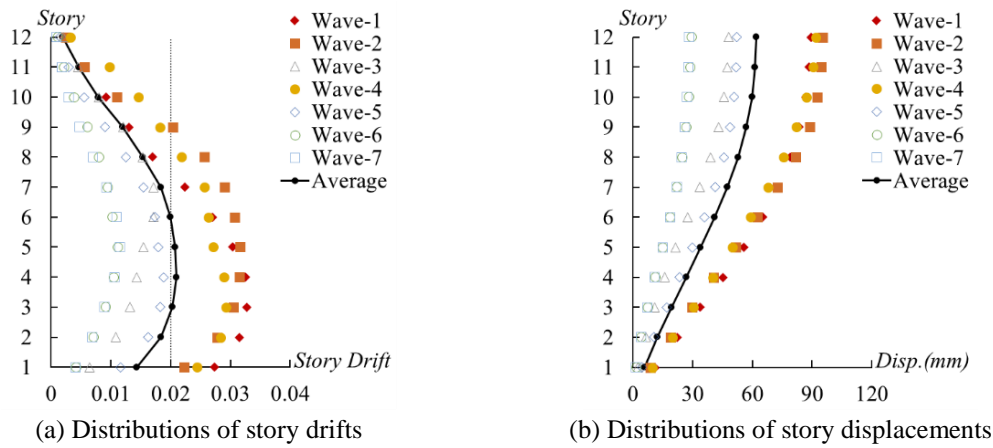


Fig. 17 Seismic responses of SWOD obtained by performing time history analysis

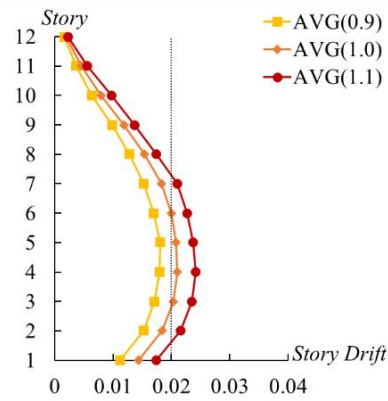
### 4.3 Verification with time history analysis

#### 4.3.1 Seismic input

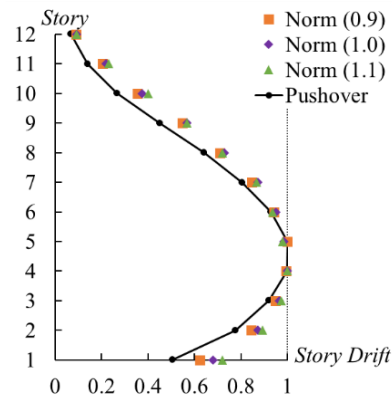
To verify the effect of the supplemental dampers, time history analysis is performed. The time histories of five natural seismic waves and two artificial seismic waves are chosen, and the details are listed in Table 4. Among these seismic waves, Nos. 1-6 are recommended by the Building Center of Japan for time history analysis (BCJ 2013), and No. 7 is a time history recorded for a building located in Tohoku University, Sendai, Japan, during the 2011 Great East Japan Earthquake (Motosaka 2011). The amplifications of the seismic waves are normalized according to their acceleration response spectrum, in which the acceleration responses at the first mode period of the structure  $T_1$  (1.07 s) are all made to be equal to that of the standard response spectrum (971.7 gal). The adjusted acceleration response spectra are shown in Fig. 16.

#### 4.3.2 Verification of damper arrangement

The distributions of the story drift and story displacement of the SWOD obtained by performing the time history analysis are shown in Fig. 17. Obvious differences can be seen among the different seismic waves. The maximum story drifts vary from approximately 0.01 to 0.03. The story drifts under seismic wave Nos. 1, 2, and 4 are relatively great, whereas those under Nos. 3, 5,

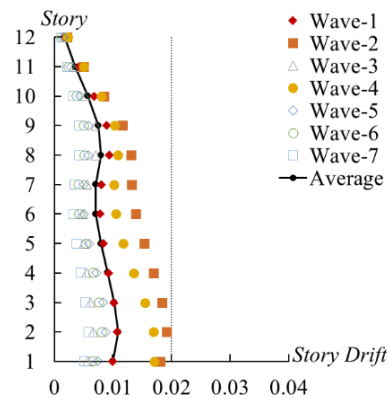


(a) Increase of the average story drifts

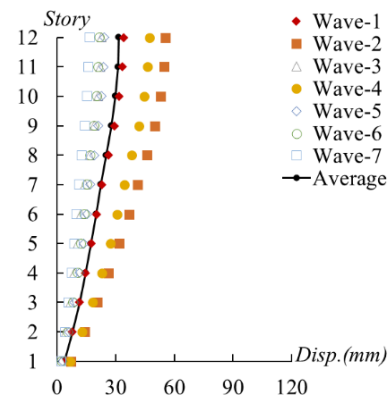


(b) Comparison with the result of pushover analysis

Fig. 18 Distribution of the average story drifts under the seismic waves multiplied by different powers



(a) Distributions of story drifts



(b) Distributions of story displacements

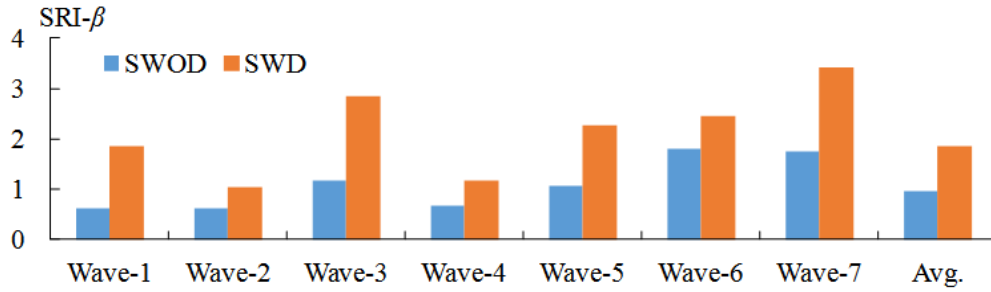
Fig. 19 Seismic responses of SWD obtained by performing time history analysis

6, and 7 are relatively small. In Fig. 16, for the range of the period that is longer than  $T_1$  (1.07 s), generally speaking, the acceleration responses of seismic wave Nos. 1, 2, and 4 are higher than those of Nos. 3, 5, 6, and 7. It can be inferred that after the structure enters the plastic range, the equivalent period becomes longer than  $T_1$ , and for the seismic waves having higher acceleration responses at the period longer than  $T_1$ , the structural responses are relatively great. In addition, it should be noted that the average of the story drifts under different seismic waves exceeds the safety limit.

To verify the selection of the installation location, the amplifications of the seismic waves used in Fig. 17 are multiplied by 0.9, 1.0, and 1.1. For each of the multiplying powers, the average story drifts of the SWOD under different seismic waves are shown in Fig. 18(a). It can be seen that Stories 2-7 have relatively great story drifts and exceed the safety limit (0.02) first, which coincides with the result obtained with Eq. (15) based on the pushover analysis (Table 2).

The average story drifts in Fig. 18(a) are normalized according to their maximum story drifts as shown in Fig. 18(b). It can be seen that the story drift distributions obtained by time history analysis and pushover analysis are almost consistent.



Fig. 20 Comparison of SRI- $\beta$  between SWOD and SWDTable 5 Comparison between SRI- $\alpha$  and SRI- $\beta$ 

Type	$d_{\max}$	$d_{\text{safe}}$	$\beta$	$\alpha$	$\beta/\alpha$	Enhancement of $\beta$	Enhancement of $\alpha$
SWOD	0.021	0.02	0.95	0.76	1.25	192%	224%
SWD	0.011	0.02	1.82	1.7	1.07		

#### 4.3.3 Verification of mitigation effect

The SWD is analyzed to verify the mitigation effect of the supplemental dampers designed according to the proposed design process. The same seismic waves are used as inputs. The distributions of the story drift and story displacement of the SWD are shown in Fig. 19. The maximum value of the average story drifts of the SWOD in Fig. 19 is 0.021, whereas that of the SWD is 0.011, which is a 48% reduction.

Considering that the safety limit state of the structure is defined according to the maximum story drift, another indicator of safety redundancy is defined based on the maximum story drift

$$\beta = \frac{d_{\text{safe}}}{d_{\max}} \quad (26)$$

where  $d_{\text{safe}}$  is the maximum story drift at the safety limit state and  $d_{\max}$  is the maximum story drift obtained by the time history analysis. For each of the seismic waves, the SRI  $\beta$  of the SWOD and SWD are compared (Fig. 20), and it can be seen that because of the supplemental dampers, the SRI  $\beta$  increases to approximately twice the original values for most of the seismic waves. The average of the SRI  $\beta$  is obtained with Eq. (33) and the SRI  $\alpha$  are compared in Table 5. The target  $\alpha$  is set to 1.7 in the design process, and the safety redundancy increases from 0.76 to 1.7 (an increase of 224%) because of the supplemental viscous dampers. At the same time, the average SRI  $\beta$  increases from 0.95 to 1.82 (an increase of 192%). That is, on average, the safety redundancy increases to approximately twice the original values, and the increase is close to the increase in the target SRI  $\alpha$ . Therefore, the performance target for a severe earthquake is satisfied by installing viscous dampers according to the design process proposed in this study.

As an example, the relationship between the damping force and actuated displacement of the damper on the left side of the fourth story (Fig. 15) under the El Centro seismic wave is shown in Fig. 21. It can be seen that the damper performs well in term of energy dissipation.

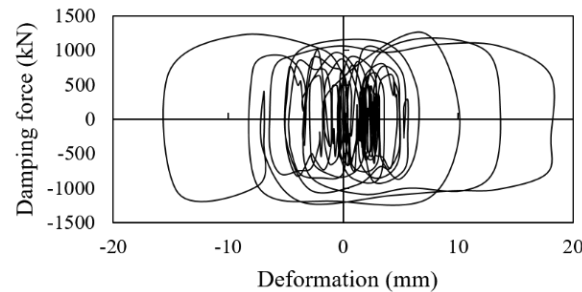


Fig. 21 Damping force-deformation relationship of one of the dampers

## 5. Conclusions

In this study, a design process is proposed for supplemental viscous dampers based on structural safety redundancy. The structural safety redundancy is evaluated by using the SRI  $\alpha$  defined in this paper. The required EDR that should be provided by the supplemental viscous dampers is determined by setting the SRI  $\alpha$  as the design target. The location and number of dampers are decided according to the distribution of the story drift obtained by performing pushover analysis, and then, the damping force and other parameters of the dampers are determined. Time history analysis is performed for a 12-story RC frame to illustrate and verify the effectiveness of the proposed design process. The results show that the performance target can be satisfied.

Compared with the elastic design process or the time history analysis, the proposed process can give better estimations of the elastic-plastic response of the structure under a severe earthquake, and higher economic efficiency can be expected. Unlike the processes based on the capacity spectrum method, the proposed process can avoid the use of iterative calculations or the graphical method and determine the required EDR by a direct calculation. Therefore, it can be concluded that the proposed process is simple and effective and has a theoretical basis, as shown in this study.

## Acknowledgements

This work was supported by the National Natural Science Foundation of China under Grant No. 51308418, and by the Shanghai Committee of Science and Technology under Grant No. 10DZ2252000.

## References

- ABCA (Australia Building Codes Board) (1996), Building code of Australia, Australia Government, Canberra.
- AIJ (Architectural Institute of Japan) (2004), Guidelines for performance evaluation of earthquake resistant reinforcement concrete buildings (draft), Tokyo, Japan. (in Japanese)
- ATC (Applied Technology Council) (1996), "Seismic evaluation and retrofit of concrete buildings", ATC-40, Redwood City, CA.

- BCJ (The Building Center of Japan) (2013), "Download of seismic waves" <http://www.bcj.or.jp/download/wave.html>. (in Japanese)
- BIA (Building Industry Authority) (1995), *The New Zealand Building Code Handbook*, Standards New Zealand, Wellington.
- Chang, K., Lin, Y. and Chen, C. (2008), "Shaking table study on displacement-based design for seismic retrofit of existing buildings using nonlinear viscous dampers", *J. Struct. Eng.*, **134**(4), 671-681.
- Chopra, A.K. (2007), *Dynamics of structures: Theory and applications to earthquake engineering*, Prentice-Hall.
- Chopra, A.K. and Goel, R.K. (1999), "Capacity-demand-diagram methods for estimating seismic deformation of inelastic structures: SDF systems", Report No. PEER-1999/02, Pacific Earthquake Engineering Research Center, University of California, Berkeley, CA.
- ECE (Economic Commission for Europe) (1996), "ECE compendium of model provisions for building regulations", United Nations Publication Sales No. E.96.IIE 4, United Nations, NY.
- Fajfar, P. (1999), "Capacity spectrum method based on inelastic demand spectra", *Earthq. Eng. Struct. Dyn.*, **28**(9), 979-993.
- FEMA (Federal Emergency Management Agency) (1997), "NEHRP guidelines for the seismic rehabilitation of buildings", FEMA-273, Applied Technology Council for the Building Seismic Safety Council, Washington D.C.
- Ghobarah, A. (2001), "Performance-based design in earthquake engineering: state of development", *Eng. Struct.*, **23**(8), 878-884.
- Gluck, N., Reinhorn, A.M., Gluck, J. and Levy, R. (1996), "Design of supplemental dampers for control of structures", *J. Struct. Eng.*, **122**(12), 1394-1399.
- Gulkan, P. and Sozen, M.A. (1974), "Inelastic responses of reinforced concrete structure to earthquake motions", *ACI J.*, **71**(12), 604-610.
- Hamidia, M., Filiatrault, A. and Aref, A. (2015), "Seismic collapse capacity-based evaluation and design of frame buildings with viscous dampers using pushover analysis", *J. Struct. Eng.*, **141**(6), 04014153.
- Huang, H.C. (2009), "Efficiency of the motion amplification device with viscous dampers and its application in highrise buildings", *Earthq. Eng. Eng. Vib.*, **8**(4), 521-536.
- Kasai, K. and Matsuda, K. (2014), "Full-scale dynamic testing of response-controlled buildings and their components: Concepts, methods, and findings", *Earthq. Eng. Eng. Vib.*, **13**(1), 167-181.
- Kim, J. and Choi, H. (2006), "Displacement-based design of supplemental dampers for seismic retrofit of a framed structure", *J. Struct. Eng.*, **132**(6), 873-883.
- Kim, J., Choi, H. and Min, K.W. (2003), "Performance-based design of added viscous dampers using capacity spectrum method", *J. Earth. Eng.*, **7**(1), 1-24.
- Lin, Y.Y., Tsai, M.H., Hwang, J.S. and Chang, K.C. (2003), "Direct displacement-based design for building with passive energy dissipation systems", *Eng. Struct.*, **25**(1), 25-37.
- Miyamoto, H.K., Gilani, A.S.J., Wada, A. and Ariyaratana, C. (2010), "Limit states and failure mechanisms of viscous dampers and the implications for large earthquakes", *Earthq. Eng. Struct. Dyn.*, **39**(11), 1279-1297.
- MLIT (Ministry of Land, Infrastructure and Transport) (1998), Revised building standard law, Kensetsu Horei Souran, Gyosei. Lmt, Tokyo, Japan.
- Motosaka, M. (2012), "Lessons of the 2011 great east Japan earthquake focused on characteristics of ground motions and building damage", *Proceedings of the International Symposium on Engineering Lessons Learned from the 2011 Great East Japan Earthquake*, Tokyo, Japan.
- Singh, M.P. and Moreshi, L.M. (2002), "Optimal placement of dampers for passive response control", *Earthq. Eng. Struct. Dyn.*, **31**(4), 955-976.
- Suarez, L.E. and Gaviria, C.A. (2015), "Dynamic properties of a building with viscous dampers in non-proportional arrangement", *Struct. Eng. Mech.*, **55**(6), 1241-1260.
- Takeda, T., Sozen, M.A. and Nielsen, N.N. (1970), "Reinforced concrete response to simulated earthquakes", *J. Struct. Div.*, **96**(12), 2557-2573.
- Weng, D.G., Zhang, C., Lu, X.L., Zeng, S. and Zhang, S.M. (2012), "A simplified design procedure for

seismic retrofit of earthquake-damaged RC frames with viscous dampers”, *Struct. Eng. Mech.*, **44**(5), 611-631.

Zhang, R. and Soong, T. (1992), “Seismic design of viscoelastic dampers for structural applications”, *J. Struct. Eng.*, **118**(5), 1375-1392.

*PL*